Versatile Like a Seahorse Tail: A Bio-Inspired Programmable Continuum Robot For Conformal Grasping

Jie Zhang, Yunge Hu, You Li, Ke Ma, Yujun Wei, Jinzhao Yang, Zhigang Wu, Hamed Rajabi,* Haijun Peng,* and Jianing Wu*

Compliant grasping is an important function of continuum robots that interact with humans and/or unpredictable environments. However, the existing robots often have cross-sections that remain constant along their length. This causes the robots to exhibit poor grasping ability, especially when dealing with objects with diverse curvatures. Here, inspired by the high adaptability of seahorse tails in grasping, a cable-driven continuum robot with tapered tensegrity, capable of conformally grasping objects with various curvatures is proposed. To characterize the effects of tapering on robotic kinematics, a mechanical model is derived using a multi-body dynamic framework for both predicting the configuration and developing a control strategy for cables. Theoretical predictions indicate that the curvature of each unit can be regulated by altering the length of the cables, allowing the robot to conform to objects with curvatures ranging from 1.48 to 28.21 m^{-1}. Further, a continuum robot is employed, and the control strategy that can be used for grasping floating objects when the curvature of the objects is used as the input is tested. The robotic design, which presents an example of embedded physical intelligence, can inspire in situ characterization techniques for collecting floating contaminants.

J. Zhang, Y. Hu, Y. Li, K. Ma, Y. Wei, J. Yang, Z. Wu, J. Wu
School of Aeronautics and Astronautics
Sun Yat-Sen University
Shenzhen 518107, P. R. China
E-mail: wujn27@mail.sysu.edu.cn

H. Rajabi
Division of Mechanical Engineering and Design
School of Engineering
London South Bank University
London SE1 0AA, UK
E-mail: rajabijh@lsbu.ac.uk

H. Peng
School of Mechanical Engineering
Dalian University of Technology
Dalian 116024, P. R. China
E-mail: hjpeng@dlut.edu.cn

The ORCID identification number(s) for the author(s) of this article can be found under https://doi.org/10.1002/aisy.202200263.

1. Introduction

Biological systems continuously inspire the development of a new class of robotic designs referred to as "continuum robots".[1,2] Compared to conventional robots composed of rigid links and joints, continuum robots, which can be characterized by their continuous core structure, known as backbone, have higher versatility,[3] greater security,[4] and stronger adaptability.[5] Hence, they can potentially be used in a variety of applications such as research and rescue,[6] minimally invasive surgery,[7] and planetary exploration.[8] Compliant grasping has recently become another interesting application for continuum robots when interacting with complex environments as well as humans.[9]

Inspired by natural hydrostats, such as elephant trunks and octopus tentacles, researchers developed continuum robots that combine soft materials with actuation patterns,[10,11] which include cable-driven,[12] pneumatic-driven,[13] and advanced materials-driven actuations.[14,15] However, a drawback of these designs is their low stiffness which can lead to detrimental large deformation when the robots encounter unpredicted loads during grasping, a phenomenon that can reduce structural stability and motion accuracy.[16] The use of a combination of both soft and rigid materials in continuum robots may resolve the conflicting requirements of structural stiffness and shape adaption, and therefore overcome the inherent drawback of the bio-inspired robots mentioned earlier.

Tensegrity structure, constructed from rigid compressive struts and flexible tensile cables, can offer an alternative building block for continuum robotic designs.[17] Recently, many typical configurations of tensegrity robots have been proposed for rolling,[18] crawling,[19] and grasping.[20] Ikemoto et al. developed a design paradigm for an arm-type tensegrity robot, which not only can mimic the characteristic of complex musculoskeletal structures but also has a better shape-preserving ability than entirely soft prototypes.[21] Zhang et al. presented a class-3 tensegrity structure to design continuum robots that can be stretched, achieving both bending and contraction patterns to enable more dexterous operations with extended reachability.[22] However, these examples had constant cross-sections along their length, which result in deformations with constant curvatures.

These design strategies hinder the adaptability of continuum robots to conformally grasp objects with various curvatures.[23–25]

To fully adapt to objects with varying curvatures that should be conformally grasped, the seahorse (hippocampus) with a square bony skeleton provides a unique inspiration source for continuum robots. The seahorses have a unique musculoskeletal geometry arranged into a few square segments, and muscles attached to the vertebra transmit forces to the bony plates to regulate the motions.[26] This square structure not only limits excessive torsion but also remains articulatory organization, which is validated to be able to hinder torsion-induced damage. In addition, the unique morphology of the seahorse tail facilities their grasping for defense and feeding.[27] Specifically, the tapered structure makes its tail become a highly maneuverable appendage,[28] to adaptively hold on to objects with a wide range of curvatures such as seagrasses and plant roots when evading predators and capturing prey.[29] However, studies have rarely focused on how to integrate the grasping adaptability of seahorse tails into the design of continuum robots, making them exhibit programmable curvature for conformal grasping of various-sized objects.

Herein, inspired by the muscular-skeleton system of the seahorse tail, we proposed a class-3 tensegrity topology for the cable-driven continuum robotic design. To elucidate the influence of tapered design on robotic conformability, we derived a mechanical model based on the multi-body dynamic methodology, which enabled us to predict the robot configuration during grasping. Taking advantage of the model, we evaluated the curvature of each unit within the robot for various tapered designs, and determined the effects of variations of the cable length on the robotic configuration. The predicted results not only revealed that this customizable control strategy can offer an effective route for highly efficient robotic manipulation and interaction, but also provide an actuation template for formulating control strategies.

We further fabricated a continuum robot consisting of ten units, using which we tested the effectiveness of the control strategies when the curvature was taken as the input. Combining with the image recognition technology, we also demonstrated that the data-driven prototype can pick up aquatic floaters, exhibiting a conformal and effective interaction with the aquatic floaters with different curvatures to help protect marine ecological environments.

2. Experimental Section

2.1. Grasping Capability of a Seahorse Tail

Seahorse is featured in its equine profile and specific swimming motion, and exhibits unique morphologies such as an elongated snout, camouflage skin, and a flexible prehensile tail, which make it become one of the remarkable sea creatures[30] (**Figure 1**a). Here, seahorse's agile tail was focused because this appendage enables the slow-moving seahorse to thrive in complex marine environments that include obstacle-strewn seagrasses, mangroves, and coral reefs.[31] To quantify the dimension of the tail, a coordinate system was built with the base of the tail as the origin O, and the longitudinal and radial directions of the tail were taken as the X-axis and Y-axis, respectively. As shown in Figure 1b, it was discovered that the seahorse tail is configured with a variable cross-section by measuring the dimension of cross-sections of the tail, and thus exhibited a specific taper, as 0.04 ± 0.01. Because of this inherent physical intelligence, they can successfully capture prey of varying shapes and dimensions, perform remarkably complex tasks, and retrieve targets from constrained environments.[32] For example, observation indicated that the seahorse tail displays the ability to hook onto objects of different dimensions, such as seagrass ($R_1 = 3.21 \pm 0.32$ mm) and branch ($R_2 = 15.35 \pm 1.43$ mm), as
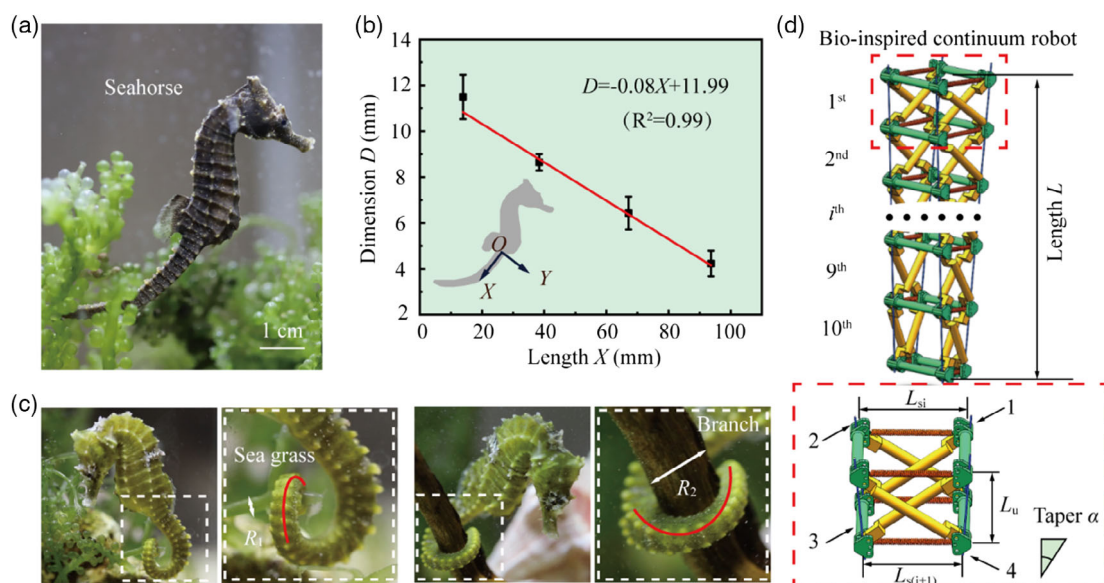

Figure 1. A bio-inspired continuum robot with varying-sized cross-sections. a) A hovering seahorse. b) Dimensions of a seahorse tail. c) A seahorse tail configuring diverse profiles for grasping various underwater objects. d) Bio-inspired continuum robot consisting of ten modular tensegrity structures. The continuum robot consists of transverse rods, longitudinal rods, springs, and cables, marked in green, yellow, red, and blue, respectively.

illustrated in Figure 1c (Video S1, Supporting Information). Because of its flexibility, agility, and adaptability for conformal grasping of a wide range of structurally various objects, the seahorse tail was selected as the model system for developing robust continuum robots.

2.2. Continuum Robotic Design

Inspired by the structural characteristics of the seahorse tail, a cable-driven continuum robot based on tensegrity structure was designed(Figure 1d). The robot was composed of n ($n = 10$) tensegrity units with an individual length of L_u, driven by four cables (No. 1–4) passing through the corresponding vertex of each unit, respectively. Each unit contained two square ring-like layers, which were alternately connected by two rigid transverse rods and two tension-loaded springs. Four longitudinal rods were divided into two groups linked to the adjacent layers by rotation hinges. Here, the lengths of transverse rods in both upper and lower layers were equal, and those of springs in the unit were L_{si} and $L_{s(i+1)}$ ($i = 1, 2..., 9$), respectively, so that the taper of the robot can be calculated as $\alpha = (L_{si} - L_{s(i+1)})/2L_u$. Moreover, four cables divided into two groups were integrated into the continuum robot for the highly maneuverable regulation of robotic configuration to reach 2D on-demand conformal grasping can be potentially accomplished in a biomimetic way.

2.3. Mechanical Model

To characterize the effects of geometrical parameters on the robotic configuration after deformation, multi-body dynamic framework was applied to build a mechanical model.[33] In this robotic system, the longitudinal and transverse rods, referred to as rigid struts, functioned as compressive components, and both springs and cables were subject to tension only. Mechanically, these were valid simplifications that allow the mechanical model to predict the robotic deformation, reducing the high computational complexity in the finite element simulation.[34] Moreover, the following assumptions were made for the cable throughout this work: 1) The contact nodes between the cable and transverse rods were fixed to the transverse rods. 2) The bending in the cables was negligible, and each segment of the cable remained straight. 3) The weight of cables and friction force between the cable and transverse rods were also negligible. Therefore, for each segment of the cable, the magnitude of the internal force was equal. 4) The cables followed a linear elastic constitutive relation. Based on these assumptions, the position vector of rigid struts and the internal force of each component were designed(Supplementary Note). Then, the components (containing $n_t = 22$ transverse rods, $n_l = 40$ longitudinal rods, $n_s = 22$ springs, and $n_c = 4$ cables) were assembled into the robotic system. Considering that the system was subjected to k boundary conditions, i.e., $\Phi(\mathbf{q}, t) \in \Re^{k \times 1}$, in which $\mathbf{q} \in \Re^{7(n_t + n_l + n_c) \times 1}$ represents the generalized coordinate vector of the system. Then, $\Phi_{\mathbf{q}}^T \lambda \in \Re^{7(n_t + n_l + n_c) \times 1}$ was introduced to describe the constraint force. In addition, the robot is actuated by the actuation criterion $f(\mathbf{q}, \mathbf{l}, t) \in \Re^{n_c \times 1}$, in which the vector $\mathbf{l} \in \Re^{n_c \times 1}$ denotes the length variation of the being pulled cables. Therefore, the general governing equations can be written as

Equation (1), and the effectiveness of this model is verified in the previous work.[22]

$$\begin{cases} \Phi_{\mathbf{q}}^T \lambda - \mathbf{Q} = \mathbf{0} \\ \Phi(\mathbf{q}, t) = \mathbf{0} \\ f(\mathbf{q}, \mathbf{l}, t) = \mathbf{0} \end{cases} \quad (1)$$

where $\Phi_{\mathbf{q}}$ and λ denote the Jacobian matrix of the boundary conditions and Lagrange multiples corresponding to the boundary conditions, respectively. $\mathbf{Q}$ is the generalized internal force vector, formulated by assembling the generalized force vector of components. $\mathbf{q}$ and $\mathbf{l}$ represent the generalized coordinate vector of the system and the length variation of the being pulled cables, respectively.

3. Results and Discussion

3.1. Effects of Robotic Taper on Curvature

We first developed a model of a typical continuum robot with a total length of 500 mm, composed of 10 units with identical cross-sections (**Figure 2**a). When shortening both cables 1 and 2 ($\Delta l_s = 100$ mm) and releasing both cables 3 and 4 ($\Delta l_r = 100$ mm), the robot can bend about the X-axis in the YOZ plane, transforming into a curved configuration with a bending angle of 120.08° from the initially straight shape. By analyzing the final curved configuration, we discovered that the curvature in each unit is approximatively equal as $\rho = 5.08 \pm 0.03 \text{ m}^{-1}$, indicating that the robot is conformal to grasp objects with this curvature.[35] However, the robot may face limitations in applicable demands, especially for adaptively grasping objects with various curvatures.[36]

To overcome this limitation, inspired by the structural characteristics of a seahorse tail, we proposed a novel design paradigm, and made a robot that can develop tapered shapes under identical actuation conditions only by regulating the length of the longitudinal rods. To reveal the influence of the tapering in grasping varying-sized objects, we developed five distinct tapers, $\alpha = 0.01$, 0.02, 0.03, 0.04, and 0.05, referred to as Cases 1–5, respectively. According to our mechanical model, the robots with different tapered designs can form various final shapes after being bent under the identical actuation criterion, as shown in Figure 2b (Video S2, Supporting Information). To evaluate deformations, we calculated the bending angle θ for each case, and found that the bending angle rises nonlinearly with the tapering α based on the following equation (Figure 2c).

$$\theta = 15.82 e^{(\alpha/0.02)} + 100.18 \quad (2)$$

Specifically, the bending angle in Case 5 reaches 352.89°, which is about three times that in Case 1, with $\theta = 127.41°$, indicating that an increased tapering increases the range of the bending angle that the robot exhibits. Therefore, a largely tapered continuum robot may demonstrate an outstanding grasping capability to firmly curl around objects like a seahorse tail.

We also calculated the bending curvature of each unit by using the least square fitting of circles, and aimed to further evaluate the adaptability of the robots to the varying-curvature objects
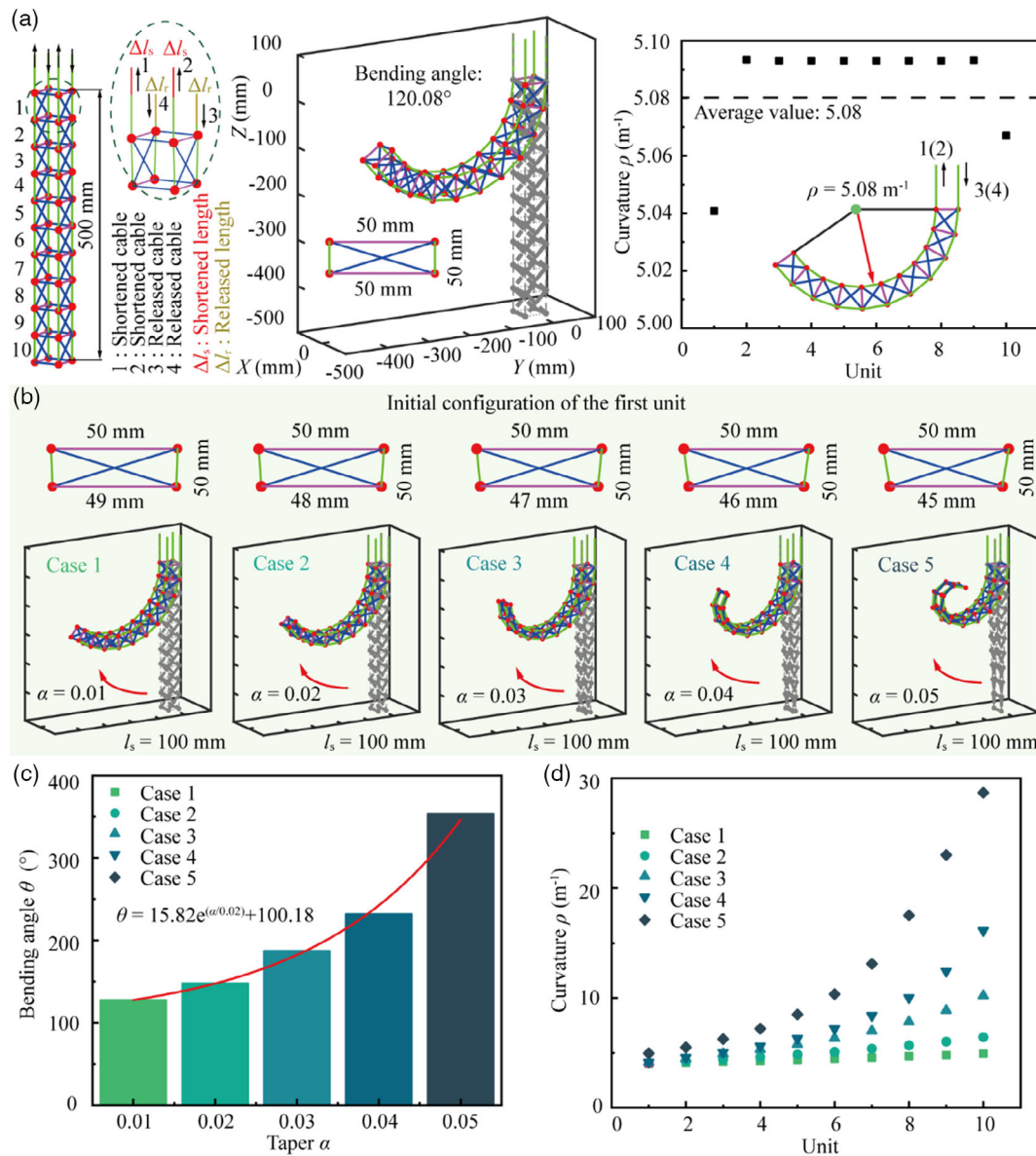
**ADVANCED
SCIENCE NEWS**

www.advancedsciencenews.com

**ADVANCED
INTELLIGENT
SYSTEMS**
Open Access

www.advintellsyst.com

Figure 2. Robotic configurations with different tapers under the same actuation criterion. a) Theoretical prediction of the bending angle and curvature for the continuum robot with a constant cross-section. b) Configuration patterns of the ten-unit continuum robot in Cases 1–5. c) Bending angle for each case. d) Effects of tapering on the curvature of each unit.

(Figure 2d). In Case 1, owing to a small taper ($\alpha = 0.01$), the curvature of each unit of the robot is basically consistent with that shown in Figure 2a, suggesting that this robot is better suited for grasping objects with a curvature ranging from 4.03 to 4.92 m^{-1}. This is a small curvature range that likely limits the usability of the robot for grasping many objects with curvatures out of this range. By contrast, although the curvature of the first unit in Case 5 is 4.95 m^{-1}, which is close to the curvature measured in Case 1, the bending curvatures display a notable variation between the units, showing a dramatic upward trend. Specifically, the curvature of the distal unit is 28.70 m^{-1}, which is about six times that of the proximal unit. Therefore, when grasping an object with small curvature, the robot can rely on basal units to conformally grasp, while the distal ones can be used to grasp objects with

larger curvature. Since the robot with a taper of $\alpha = 0.05$ can achieve a more conformal grasping toward the varying-curvature objects, compared with other ones, we adopted the robot in Case 5 as an ideal configuration for further analysis.

3.2. Robot Configurations with Respect to Cable Length Variations

Another factor that influences the configuration of our continuum robot is the lengths of the cables used for actuation. Hence, we evaluated the effects of the cable length on the curvature of the robot for the condition under which the length variation of cables satisfies the actuation criterion 1 of
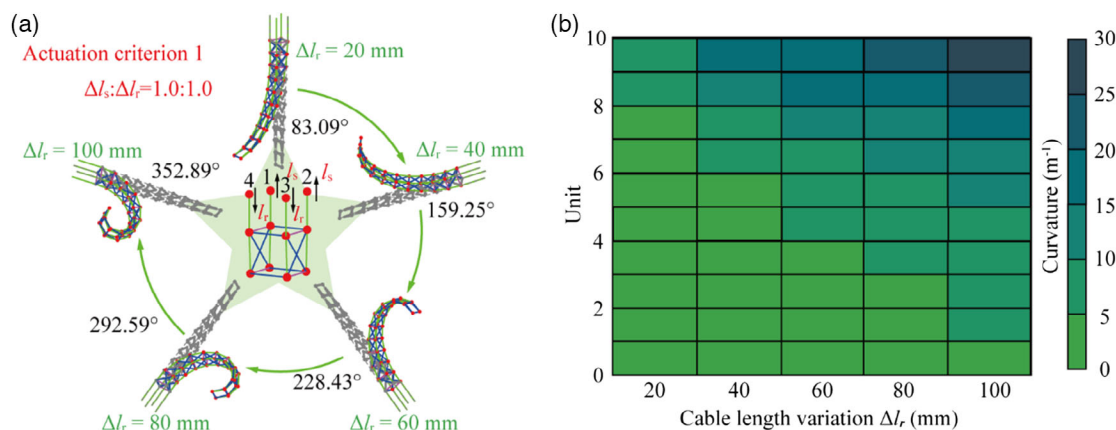
ADVANCED
SCIENCE NEWS

www.advancedsciencenews.com

ADVANCED
INTELLIGENT
SYSTEMS
Open Access

www.advintellsyst.com

Figure 3. Effects of cable length variation on robotic curvature. a) Snapshots of the theoretical robotic profiles when cable length variations satisfy the Actuation Criterion 1. b) Changes of curvature of each unit by the cable length variation.

$\Delta l_s : \Delta l_r = 1.0 : 1.0$. Here, Δl_s and Δl_r represent the shortened and released length variations, respectively. Under this criterion, we shortened Cables 1 and 2 from 20 to 100 mm, respectively, and obtained the corresponding bending profiles of the robot. The relationship of the bending angle and the cable length variations, obtained from our theoretical investigation, is depicted in **Figure 3**a. To test the conformability of the robot to objects, we also calculated the curvature of each unit, based on which

we mapped the results in Figure 3b. Taking the distal unit as an example, we found that the curvature of the unit increases by 358.18% when the cable length is increased from 20 to 100 mm, indicating that the robot can be more adapted to grasp smaller objects by shortening both Cables 1 and 2. This physical intelligence facilitates the adaptability of continuum robots for varying-curvature objects, overcoming the obstacle of curvature mismatching in grasping.
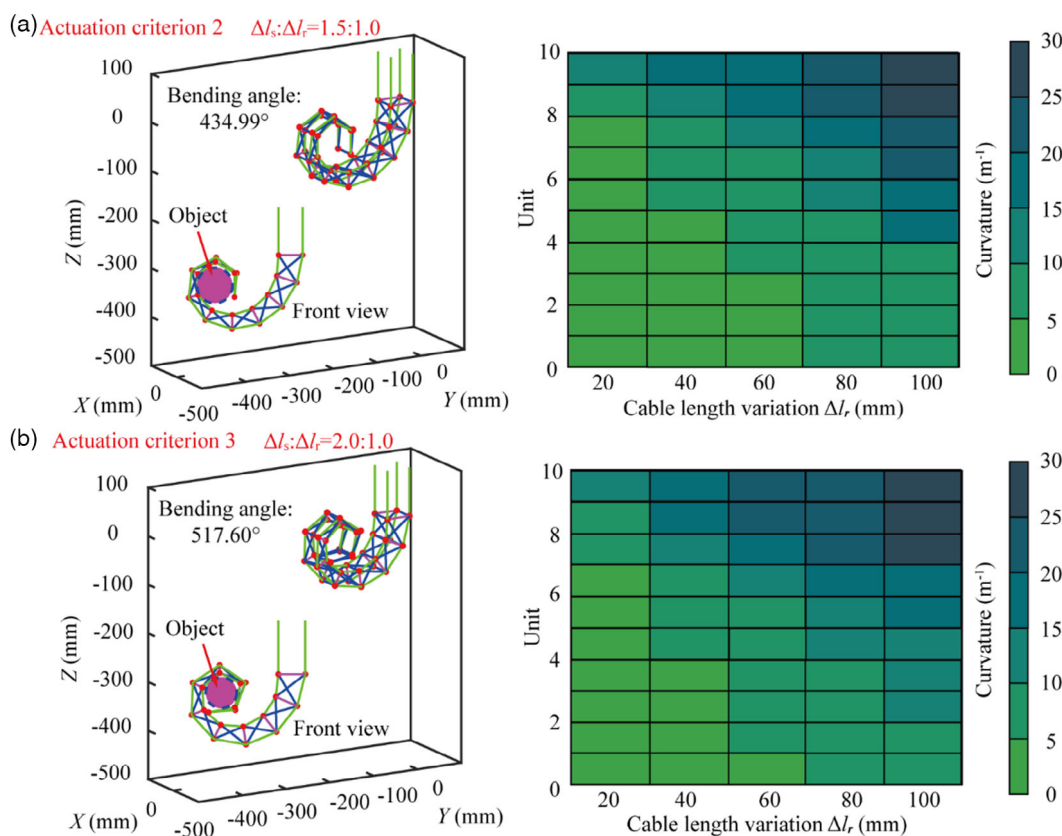

Figure 4. Relationship between the cable length on robotic curvature. a) Actuation Criterion 2: $\Delta l_s : \Delta l_r = 1.5 : 1.0$. Influence of the length variation and unit position on the curvature in Criterion 2. b) Actuation Criterion 3: $\Delta l_s : \Delta l_r = 2.0 : 1.0$. Influence of length variation and unit position on the curvature in Criterion 3.

Our mapping also provides a curvature library that allows for formulating the control strategies for cables according to the expected curvatures. For example, to grasp objects with 5–10 m^{-1} curvatures, we should shorten both Cables 1 and 2 by 60 mm, and release Cables 3 and 4 for an equal length to enhance the curvature consistency between the robot and the object. However, a single actuation criterion may lead to a mismatch between the bending curvature of the robot and that of the objects, or even cause grasping failure. Therefore, it is necessary to further enrich the applicable control mapping for the regulation of robotic profiles.

To enhance the conformability of the robot for on-demand grasping varying-curvature objects, we proposed two other criteria to enrich the library by regulating the ratio ξ between shortening and releasing the length of cables (**Figure 4**). By comparing the results under these criteria, we found that the maximum curvature reaches 28.21 m^{-1} in Criterion 3, showing an increase of

22.49% and 7.88% compared with Criteria 1 and 2. This result suggests that, by increasing the ratio ξ, the robot can display higher adaptability to objects with large curvatures. Considering that these criteria have different applicable curvature intervals, we should accurately select the corresponding mapping to satisfy the geometrical requirements of conformal grasping. Therefore, the control strategies of the cables can be determined by taking the curvature as the input, and the deployment can be delicately designed to conform to the varying-size objects.

3.3. Application Demonstration

To explore and demonstrate the applications of the programmable curvature, we fabricated a tapered continuum robot consisting of ten units, and mounted the first unit on a rigid robotic arm (SJ 602-A, Anno, China), as illustrated in **Figure 5**a. The robot
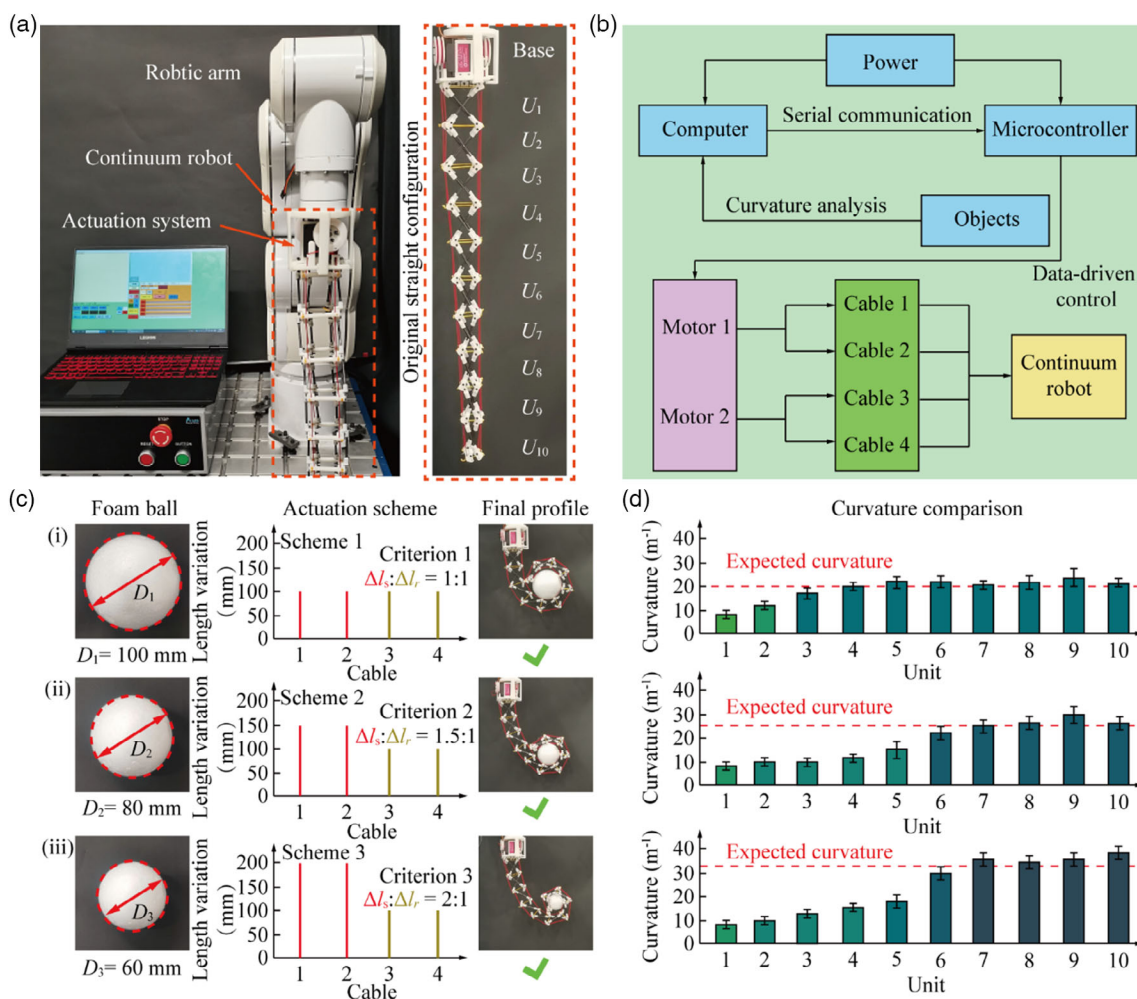

Figure 5. Performance of the continuum robot in grasping foam balls with different curvatures. a) Experimental setup consisting of a rigid robotic arm and the continuum robot. The original configuration of the robot with 10 vertically aligned units (U_1 to U_{10}). b) The control system for the continuum robot. c) Final profiles of conformal grasping. Three actuation schemes are used to drive the continuum robot, enabling it to conformally grasp foam balls with diameters of $D_1 = 100$ mm, $D_2 = 80$ mm, and $D_3 = 60$ mm, respectively. d) Comparisons of the expected and actual robotic curvatures under the three actuation schemes, respectively.

is actuated by four cables pulled by two motors (RDS3115, DS-Servo, China), all of which are controlled by a microcontroller (Arduino UNO, Arduino, Germany) (Figure 5b). To exhibit the conformal property of our continuum robot for grasping varying-curvature objects, we prepared foam balls in diameters of 60, 80, and 100 mm, respectively, as shown in Figure 5c. Here, we demonstrated that the effective curvature can be programmed based on the library to achieve conformal grasping. Specifically, we first calculated the contour curvature of the foam ball with a diameter of 100 mm (i.e., $\rho_1 = 20.00\,\text{m}^{-1}$), based on which Criterion 1 is selected as the actuation scheme. When both Cables 3 and 4 are released for 100 mm, the robot can turn around the foam ball, analogously to a seahorse tail grasping a branch. To further analyze the interaction between the robot and foam ball, we measured the curvature of each unit, and found that the curvature from Unit 4 to Unit 10 is approximately consistent with the expected curvature ($\rho_1 = 20.00\,\text{m}^{-1}$). This indicates that this actuation scheme can enable the robot to achieve on-demand conformal grasping. Similarly, for the other two types of foam balls, we also formulated the corresponding actuation schemes according to their contour curvatures, and the experimental trials also show the good conformality between the robot and objects, indicating that the robot can grasp objects in different sizes through programmable curvature given in the library.

We also measured the energy consumption for the grasping actions using $W = l_{sum}P/2\pi R\omega$, where l_{sum} and R represent the cable length variation and radius of the coil, respectively. P and ω

are the rated power and speed of the motor, respectively (**Table 1**). Specifically, when grasping the ball with a diameter of 60 mm ($\rho_3 = 33.33\,\text{m}^{-1}$), the robotic system can only adopt one scheme to realize conformal grasping, during which 47.77 J energy is consumed (**Figure 6**a). However, for some other curvature requirements, more than one actuation scheme can be used to achieve a conformal grasp as the corresponding cable control strategy may be found in each mapping. For example, for the foam ball with a diameter of 100 mm ($\rho_1 = 20.00\,\text{m}^{-1}$), the robot can grasp the ball conformally under the three actuation schemes, as shown in Figure 6b. By comparing the energy consumed under each of these schemes, we discovered that Scheme 1 consumes only 31.85 J, which is 80.01% and 66.67% of energy consumption under the other two schemes, respectively. Therefore, Scheme 1 is more optimal than the others. This suggests that a tradeoff between conformality and energy consumption can be used to determine the actuation strategy of the cables.

The data-driven robot is evaluated for picking up the aquatic floating objects, including a Coke can, a potato chips jar, and a sesame seed bucket (Video S3, Supporting Information). We adjusted the width of the tank using an acrylic board to make the objects loosely constrained along their long axis, to improve the focus for recordings. For the robot to be able to grasp these objects, we first extracted their sectional curvature by image contour extraction ($\rho_1 = 35.88 \pm 0.69$, $\rho_2 = 30.31 \pm 0.38$, and $\rho_3 = 19.83 \pm 0.61\,\text{m}^{-1}$), based on which the control strategies of the cables can be determined, and then refer to the control flow in Figure S3, Supporting Information. The results demonstrate that the robot can grasp the objects conformably (**Figure 7**). To evaluate the grasping performance of the robot, we compared the curvature of the robotic profile with that of the objects, and discovered that the maximum error between the expected and the real robotic curvatures is only 15.32%. This good agreement indicates that the robot has a favorable ability to interact with the floating objects of known curvature, which may inspire a variety of in situ characterization techniques used to collect floating contaminants in the future.

Table 1. Physical properties of the components.

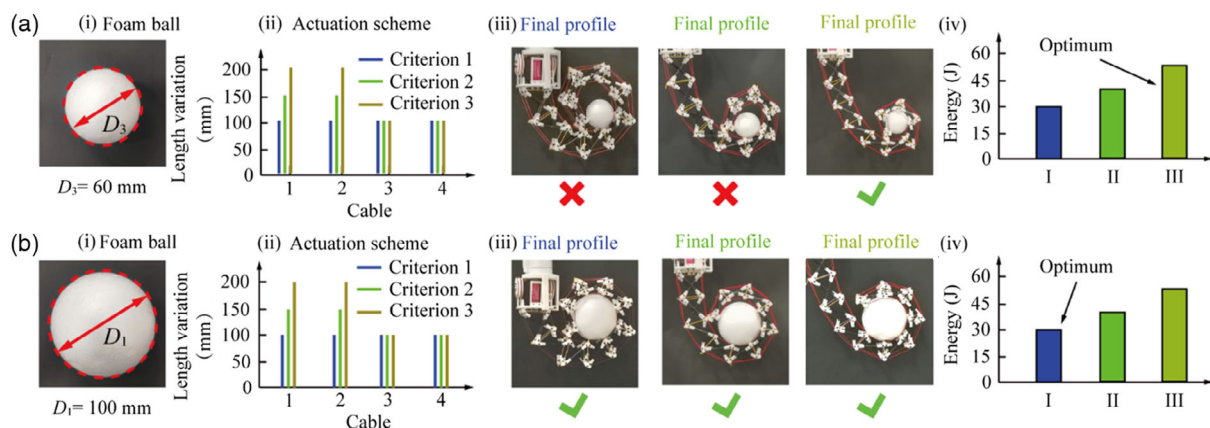| No.	Parameter	Value
1	Cable length variation l_{sum} [mm]	$l_s + l_r$
2	Radius of the coil R [mm]	15.00
3	Rated power P [W]	15.00
4	Rated speed ω [rad s^{-1}]	1.26

Figure 6. Energy consumption under the different actuation schemes. a) Selection of the actuation strategy for conformal grasping. b) Optimal actuation scheme under the principle of minimum consumed energy. i) Outline of foam balls. ii) Actuation schemes for varying curvatures. iii) Final profiles under three diverse actuation schemes. iv) Comparison of energy consumption for actuating motors.
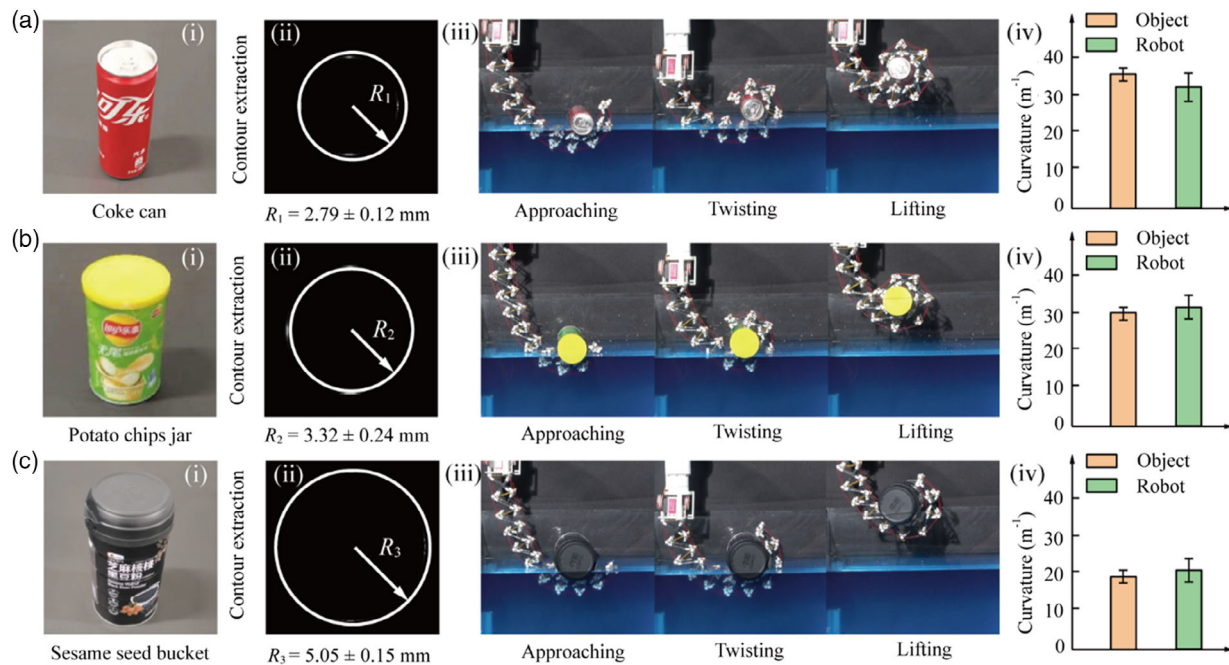
Figure 7. Bionic continuum robot picking up aquatic floating objects. R_i ($i = 1, 2, 3$) represents sectional curvatures of floating objects. Comparison of the objects and actual robotic curvatures. a) Coke can. b) Potato chips jar. c) Sesame seed bucket. i) Floating objects with varying curvatures. ii) Contour extraction of the floating objects. iii) Snapshots of the conformal grasping for varying curvatures. iv) Comparison of curvatures for actuating motors.

4. Conclusion

Inspired by the structural characteristics of the seahorse tail, we presented a tapered tensegrity structure for cable-driven continuum robots. Leveraging inherent physical intelligence, this robotic system can conformally grasp objects in various curvatures. Our design not only offers an effective route for efficient robotic interaction but can be an effective solution for the customization of continuum robots through programming output curvature. Continuum robots developed using our design can be used, for example, for cleaning rivers from floating objects. Future works should focus on equipping our design with flexible sensors to allow firm grasping of objects through real-time monitoring of the grasping force.[37]

Supporting Information

Supporting Information is available from the Wiley Online Library or from the author.

Conflict of Interest

The authors declare no conflict of interest.

Author Contributions

Z.W., H.P., and J.W.: conceived the concept; J.Z., Y.W., and J.Y.: performed the simulations; J.Z., Y.L., M.K., and Y.H.: carried out experiments and data processing; J.Z., H.R., and J.W.: analyzed the data and interpreted the results; H.R., H.P., and J.W.: directed the project. All authors commented on the article.

Data Availability Statement

The data that support the findings of this study are available in the supplementary material of this article.

[1] D. Trivedi, C. D. Rahn, W. M. Kier, I. D. Walker, *Appl. Bionics Biomech.* **2008**, *5*, 99.

[2] C. Majidi, *Soft Rob.* **2014**, *1*, 5.

[3] J. Santoso, C. D. Onal, *Soft Rob.* **2021**, *8*, 371.

[4] J. D. Greer, T. K. Morimoto, A. M. Okamura, E. W. Hawkes, in *2017 IEEE Int. Conf. on Robotics and Automation (ICRA)*, IEEE, Piscataway, NJ **2017**, pp. 5503–5510.

[5] B. Chen, Z. Shao, Z. Xie, J. Liu, F. Pan, L. He, L. Zhang, Y. Zhang, X. Ling, F. Peng, W. Yun, L. Wen, *Adv. Intell. Syst.* **2021**, *3*, 2000251.

[6] T. Tolley Michael, F. Shepherd Robert, C. Galloway Kevin, J. Wood Robert, M. Whitesides George, *Soft Rob.* **2014**, *1*, 213.

[7] Y. Chen, B. Wu, J. Jin, K. Xu, *IEEE Rob. Autom. Lett.* **2021**, *6*, 1590.

[8] N. G. Tsagarakis, D. G. Caldwell, *Auton. Rob.* **2003**, *15*, 21.

[9] K. C. Galloway, K. P. Becker, B. Phillips, J. Kirby, S. Licht, D. Tchernov, R. J. Wood, D. F. Grube, *Soft Rob.* **2016**, *3*, 23.

[10] B. A. Jones, I. D. Walker, *IEEE Trans. Rob.* **2006**, *22*, 43.

[11] T. Zheng, D. T. Branson, E. Guglielmino, R. Kang, G. A. Medrano Cerda, M. Cianchetti, M. Follador, I. S. Godage, D. G. Caldwell, *J. Mech. Rob.* **2013**, *5*, 021004.

[12] C. Sun, L. Chen, J. Liu, J. S. Dai, R. Kang, *Proc. Inst. Mech. Eng. Part C* **2020**, *234*, 318.

[13] W. Hu, G. Alici, *Soft Rob.* **2020**, *7*, 267.

[14] Z. Xing, J. Zhang, D. McCoul, Y. Cui, L. Sun, J. Zhao, *Soft Rob.* **2020**, *7*, 512.

[15] Y. Yue, Q. Wang, Z. Ma, Z. Wu, X. Zhang, D. Li, Y. Shi, B. Su, *Soft Rob.* **2022**.

[16] M. Shan, J. Guo, E. Gill, *Prog. Aerosp. Sci.* **2016**, *80*, 18.

[17] D. S. Shah, J. W. Booth, R. L. Baines, K. Wang, M. Vespignani, K. Bekris, R. Kramer-Bottiglio, *Soft Rob.* **2021**, *5*, 639.

[18] J. W. Booth, O. Cyr-Choiniere, J. C. Case, D. Shah, M. C. Yuen, R. Kramer-Bottiglio, *Soft Rob.* **2021**, *8*, 531.

[19] M. Chen, J. Liu, R. E. Skelton, *Mech. Res. Commun.* **2020**, *103*, 103480.

[20] W.-Y. Li, H. Nabae, G. Endo, K. Suzumori, *IEEE Rob. Autom. Lett.* **2020**, *5*, 4345.

[21] S. Ikemoto, K. Tsukamoto, Y. Yoshimitsu, *Front. Rob. AI* **2021**, *8*.

[22] J. Zhang, Z. Kan, Y. Li, Z. Wu, J. Wu, H. Peng, *IEEE Rob. Autom. Lett.* **2022**, *7*, 6163.

[23] J. Liu, T. Jin, L. Li, F. Yang, Y. Tian, Y. Xian, F. Xi, *2018 IEEE Int. Conf. on Robotics and Biomimetics (ROBIO)*, IEEE, Piscataway, NJ **2018**, pp. 361–366.

[24] Z. Chai, L. Lyu, M. Pu, X. Chen, J. Zhu, H. Liang, H. Ding, Z. Wu, *Adv. Intell. Syst.* **2022**, 2100262.

[25] L. Li, T. Jin, Y. Tian, F. Yang, F. Xi, *IEEE Access* **2019**, *7*, 57151.

[26] M. M. Porter, E. Novitskaya, A. B. Castro-Ceseña, M. A. Meyers, J. McKittrick, *Acta Biomater.* **2013**, *9*, 6763.

[27] S. Van Wassenbergh, G. Roos, L. Ferry, *Nat. Commun.* **2011**, *2*.

[28] T. Praet, D. Adriaens, S. V. Cauter, B. Masschaele, M. D. Beule, B. Verhegghe, *Int. J. Numer. Methods Biomed. Eng.* **2012**, *28*, 1028.

[29] D. Kleiber, L. Blight, I. Caldwell, A. Vincent, *Rev. Fish Biol. Fish.* **2011**, *21*, 205.

[30] S. A. Foster, A. C. Vincent, *J. Fish Biol.* **2004**, *65*.

[31] S. A. Lourie, A. C. Vincent, H. J. Hall, *Seahorses: An Identification Guide to the World's Species and their Conservation*, Project Seahorse, London UK **1999**.

[32] M. E. Hale, *J. Morphol.* **1996**, *227*, 51.

[33] Z. Kan, H. Peng, B. Chen, W. Zhong, *Int. J. Solids Struct.* **2018**, *130*, 61.

[34] H. Peng, N. Song, F. Li, S. Tang, *J. Appl. Mech.* **2022**, *89*, 071005.

[35] D. Lin, J. Wang, N. Jiao, Z. Wang, L. Liu, *Adv. Intell. Syst.* **2021**, *3*, 2000211.

[36] X. Ke, J. Jang, Z. Chai, H. Yong, J. Zhu, H. Chen, C. F. Guo, H. Ding, Z. Wu, *Soft Rob.* **2021**.

[37] Z. Ma, Q. Wang, Z. Wu, D. Chen, C. Yan, Y. Shi, M. D. Dickey, B. Su, *Adv. Mater.* **2022**, *34*, 2203814.